International Journal of Solids and Structures 47 (2010) 1381–1391

Contents lists available at ScienceDirect

International Journal of Solids and Structures

journal homepage: www.elsevier.com/locate/ijsolstr

Fracture analysis in continuously nonhomogeneous magneto-electro-elastic solids under a thermal load by the MLPG

J. Sladek [a,*], V. Sladek [a], P. Solek [b], Ch. Zhang [c]

[a] Institution of Construction and Architecture, Slovak Academy of Sciences, 84503 Bratislava, Slovakia
[b] Department of Mechanics, Slovak Technical University, Bratislava, Slovakia
[c] Department of Civil Engineering, University of Siegen, D-57068 Siegen, Germany

ARTICLE INFO

Article history:
Received 3 July 2009
Received in revised form 11 December 2009
Available online 11 February 2010

Keywords:
Meshless local Petrov–Galerkin method (MLPG)
Moving least-squares approximation
FGM
2D problems
Internal and edge cracks
Houbolt method

ABSTRACT

A meshless method based on the local Petrov–Galerkin approach is proposed, to solve initial-boundary value problems of magneto-electro-elastic solids with continuously varying material properties. Stationary and transient thermal problems are considered in this paper. The mechanical 2-D fields are described by the equations of motion with an inertial term. Nodal points are spread on the analyzed domain, and each node is surrounded by a small circle for simplicity. The spatial variation of displacements, electric and magnetic potentials is approximated by the moving least-squares (MLS) scheme. After performing the spatial integrations, one obtains a system of ordinary differential equations for certain nodal unknowns. That system is solved numerically by the Houbolt finite-difference scheme as a time stepping method.

1. Introduction

Magneto-electro-elastic materials have the ability of converting the energy from one type to other (among magnetic, electric, and mechanical) (Avellaneda and Harshe, 1994; Berlingcourt et al., 1964; Landau and Lifshitz, 1984; Nan, 1994). This behaviour is extensively utilized in construction of transducers, sensors and actuators for smart structures. Earlier research activities were focused on modeling magneto-electro-elastic fields (Alshits et al., 1992; Chung and Ting, 1995; Huang and Kuo, 1997; Li, 2000; Pan, 2001; Liu et al., 2001; Wang and Shen, 2002). Unfortunately, magneto-electro-elastic materials are brittle and they have a tendency to develop cracks even in manufacture process. Therefore, it is important to understand fracture of magneto-electro-elastic materials (Beom and Atluri, 2003; Gao et al., 2003; Song and Sih, 2003; Zhou et al., 2004; Hu et al., 2006; Wang et al., 2006; Tian and Gabbert, 2005; Tian and Rajapakse, 2005; Garcia-Sanchez et al., 2007b; Wang and Mai, 2007). Applications are mostly made under a static deformation assumption. Dynamic fracture analyses are considered very seldom in the literature.

While the piezoelectric and piezomagnetic effects are due to electro-elastic and magneto-elastic interactions, respectively, the magnetoelectric effect is the induction of the electrical polarization by magnetic field and the induction of magnetization by electric field via electro-magneto-elastic interactions. Magnetoelectric coupling plays an important role in the dynamic behaviour of certain materials, especially compounds which possess simultaneously ferroelectric and ferromagnetic phases (Eringen and Maugin, 1990). The electric and magnetic symmetry groups for certain crystals permit the piezoelectric and piezomagnetic as well as magnetoelectric effects. In centrosymmetric crystals neither of these effects exists. Some composite materials can provide superior properties compared to their constituents. The magneto-electro-mechanical coupling in some composites can be hundred times higher than in single-phase materials (Nan, 1994; Feng and Su, 2006; Tong et al., 2008). Therefore, the multi-field coupling has to be considered in mathematical modeling. If the volume fraction of constituents is varying in a predominant direction, we are talking about functionally graded materials (FGMs). Originally these materials have been introduced to benefit from the ideal performance of its constituents, e.g. high heat and corrosion resistance of ceramics on one side, and large mechanical strength and toughness of metals on the other side. A review on various aspects of FGMs can be found in the monograph of Suresh and Mortensen (1998). Later, the demand for piezoelectric materials with high strength, high toughness, low thermal expansion coefficient and low dielectric constant encourages the study of functionally graded piezoelectric materials (Zhu et al., 1995; Han et al., 2006). According to the best of authors' knowledge there is only one paper available (Feng and Su, 2006) with applications to continuously nonhomogeneous magneto-electric materials.

* Corresponding author. Tel.: +421 2 54 788 662.
E-mail address: sladek@savba.sk (J. Sladek).

0020-7683/$ - see front matter © 2010 Elsevier Ltd. All rights reserved.
doi:10.1016/j.ijsolstr.2010.01.025

Certain piezoelectric and magneto-electro-elastic materials are also temperature sensitive, i.e. an electric charge or voltage is generated when temperature variations are exposed. This effect is called the pyroelectric effect. If a temperature load is considered in a magneto-electro-elastic solid, it is needed to take into account a coupling of magneto-electro-thermo-mechanical fields. The theory of thermo-piezoelectricity was proposed for the first time by Mindlin (1974). The physical laws for thermo-piezoelectric materials have been explored by Nowacki (1978). Recently, the authors have analyzed piezoelectric materials under a thermal load (Sladek et al., 2007b).

The solution of general boundary value problems for continuously nonhomogeneous magneto-electro-elastic solids requires advanced numerical methods due to the high mathematical complexity. Such a multi-field problem is described by a system of partial differential equations because of the interactions among the magnetic, electric and mechanical fields involved in the constitutive equations. Therefore, the number of literature sources on the problem is very limited. Drobenko et al. (2008) developed a mathematical model for coupled time-dependent electromagnetic, thermal and mechanical processes, which occur in polarizable and magnetizable electroconductive solids subjected to an electromagnetic field. Zhu and Qin (2007) applied the hypersingular integral equation method to crack problems in electro-magneto-thermo-elastic multiphase composites. He and Li (2006) have solved electro-magneto-thermo-elastic problem for a half-space. In spite of the great success of the finite element method (FEM) and boundary element method (BEM) as effective numerical tools for the solution of boundary value problems in mainly elastic solids, there is still a growing interest in the development of new advanced numerical methods. In recent years, meshless formulations are becoming popular due to their high adaptability and low costs to prepare input and output data in numerical analysis. The moving least-squares (MLS) approximation is generally considered as one of many schemes to interpolate discrete data with a reasonable accuracy. The order of continuity of the MLS approximation is given by the minimum between the orders of continuity of the basis functions and that of the weight function. So continuity can be tuned to a desired value. In conventional discretization methods, the interpolation functions usually result in a discontinuity of secondary fields (gradients of primary fields) on the interfaces of elements. For modeling of continuously nonhomogeneous solids the approach based on piecewise continuous elements can bring some inaccuracies. Therefore, modeling based on C^1-continuity, such as in meshless methods, is expected to be more accurate than conventional discretization techniques. The meshless or generalized FEM methods are also very convenient for modeling of cracks. One can embed particular enrichment functions at the crack-tip so the stress intensity factor can be predicted accurately (Fleming et al., 1997).

A variety of meshless methods has been proposed so far, with some of them being applied only to piezoelectric problems (Ohs and Aluru, 2001; Liu et al., 2002). They can be derived from a weak-form formulation either on the global domain or on a set of local subdomains. In the global formulation, background cells are required for the integration of the weak-form. In methods based on local weak-form formulation, no background cells are required and therefore they are often referred to as truly meshless methods. The meshless local Petrov–Galerkin (MLPG) method is a fundamental base for the derivation of many meshless formulations, since the trial and test functions can be chosen from different functional spaces (Zhu et al., 1998; Atluri et al., 2000; Sladek et al., 2000, 2001, 2003a,b; Sellountos et al., 2005). Recently, the MLPG method with a Heaviside step function as the test functions (Atluri et al., 2003; Sladek et al., 2004, 2006a) has been applied to solve two-dimensional (2-D) homogeneous and continuously nonhomogeneous piezoelectric solids (Sladek et al., 2006b, 2007a,b). Present authors have recently analyzed dynamic 3-D axisymmetric problems in continuously nonhomogeneous piezoelectric solids (Sladek et al., 2008).

In this paper, the MLPG method is applied to 2-D continuously nonhomogeneous magneto-electro-elastic solids subjected to thermal loadings. Stationary and transient thermal loads are considered here. The coupled governing partial differential equations are satisfied in a weak-form on small fictitious subdomains. Nodal points are introduced and spread on the analyzed domain and each node is surrounded by a small circle for simplicity, but without loss of shape generality. For a simple shape of subdomains, such as a circle used in this paper, numerical integrations over them can be easily carried out. The integral equations have a very simple nonsingular form. The spatial variations of the displacements, electric and magnetic potentials are approximated by the moving least-squares scheme (Belytschko et al., 1996; Atluri, 2004). After performing the spatial integrations, one obtains a system of ordinary differential equations for certain nodal unknowns. That system is solved numerically by the Houbolt finite-difference scheme (Houbolt, 1950) as a time stepping method. The accuracy and the efficiency of the proposed MLPG method are verified by several numerical examples for central and edge cracks.

2. Local boundary integral equations

The governing equations of the phenomenological theory of magneto-electro-elastic materials under a thermal load consist of Maxwell's equations, the heat conduction equation and the balance of momentum. The governing equations, which are complemented by the boundary and initial conditions, should be solved for the unknown primary field variables such as the elastic displacement vector field $u_i(\mathbf{x},\tau)$, the electric potential $\psi(\mathbf{x},\tau)$ (or its gradient, called the electric vector field $E_i(\mathbf{x},\tau)$), the magnetic potential $\mu(\mathbf{x},\tau)$ (or its gradient, called the magnetic intensity field $H_i(\mathbf{x},\tau)$), and temperature $\theta(\mathbf{x},\tau)$. The constitutive equations correlate the primary fields $\{u_i, E_i, H_i, \theta\}$ with the secondary fields $\{\sigma_{ij}, D_i, B_i, q\}$, which are the stress tensor field, the electric displacement vector field, the magnetic induction vector field, and the heat flux, respectively. The governing equations give not only the relationships between conjugated fields in each of the pairs $(\sigma_{ij},\varepsilon_{ij})$, (D_i,E_i), (B_i,H_i), (θ,q) but describe also the electro-magneto-thermo-elastic interactions in the phenomenological theory of continuous solids.

Taking into account the typical material coefficients, it can be found that the characteristic frequencies for thermal, elastic and electromagnetic processes are $f_{\text{th}} = 10^{-3}$ Hz, $f_{\text{el}} = 10^{4}$ Hz and $f_{\text{elm}} = 10^{7}$ Hz, respectively. Thus, if we consider such bodies under transient loadings, with temporal changes corresponding to f_{th} and/or f_{el}, the changes of the electromagnetic fields can be assumed to be immediate, or in other words the electromagnetic fields can be considered like quasi-static (Parton and Kudryavtsev, 1988). Then, the Maxwell equations are reduced to two scalar equations

$$D_{j,j}(\mathbf{x},\tau) = 0, \tag{1}$$

$$B_{j,j}(\mathbf{x},\tau) = 0. \tag{2}$$

The rest of the vectorial Maxwell's equations in quasi-static approximation, $\nabla \times \mathbf{E} = 0$ and $\nabla \times \mathbf{H} = 0$, are satisfied identically by an appropriate representation of the fields $\mathbf{E}(\mathbf{x},\tau)$ and $\mathbf{H}(\mathbf{x},\tau)$ as gradients of scalar electric and magnetic potentials $\psi(\mathbf{x},\tau)$ and $\mu(\mathbf{x},\tau)$, respectively,

$$E_j(\mathbf{x},\tau) = -\psi_{,j}(\mathbf{x},\tau), \tag{3}$$
$$H_j(\mathbf{x},\tau) = -\mu_{,j}(\mathbf{x},\tau). \tag{4}$$

To complete the set of governing equations, Eqs. (1) and (2), one needs to use the equations of motion and the heat conduction in an elastic continuum

$$\sigma_{ij,j}(\mathbf{x},\tau) + X_i(\mathbf{x},\tau) = \rho\ddot{u}_i(\mathbf{x},\tau), \tag{5}$$
$$\left[k_{ij}(\mathbf{x})\theta_{,j}(\mathbf{x},\tau)\right]_{,i} - \rho(\mathbf{x})c(\mathbf{x})\dot{\theta}(\mathbf{x},\tau) = 0, \tag{6}$$

where $\ddot{u}_i$, ρ and X_i denote the acceleration of displacements, the mass density, and the body force vector, respectively. Also, k_{ij} and c are the thermal conductivity tensor and specific heat, respectively. A comma after a quantity represents the partial derivatives of the quantity and a dot is used for the time derivative. Recall that the acceleration term is usually omitted in a quasi-static approximation when the transient thermal loadings change with a characteristic frequency f_{th}. Nevertheless, we consider this term in order to incorporate elastic waves into simulations of processes under thermal shocks. On the other hand, the influence of the time derivatives of the displacement and electro-magnetic fields on the heat conduction is neglected because of the significant differences in the characteristic frequencies.

Finally, we assume the constitutive equations involving the general electro-magneto-thermo-elastic interaction (Huang and Kuo, 1997) for continuously non-homogeneous media with spatially dependent material coefficients

$$\sigma_{ij}(\mathbf{x},\tau) = c_{ijkl}(\mathbf{x})\varepsilon_{kl}(\mathbf{x},\tau) - e_{kij}(\mathbf{x})E_k(\mathbf{x},\tau) - d_{kij}(\mathbf{x})H_k(\mathbf{x},\tau) - \lambda_{ij}(\mathbf{x})\theta(\mathbf{x},\tau), \tag{7}$$

$$D_j(\mathbf{x},\tau) = e_{jkl}(\mathbf{x})\varepsilon_{kl}(\mathbf{x},\tau) + h_{jk}(\mathbf{x})E_k(\mathbf{x},\tau) + \alpha_{jk}(\mathbf{x})H_k(\mathbf{x},\tau) + p_j(\mathbf{x})\theta(\mathbf{x},\tau), \tag{8}$$

$$B_j(\mathbf{x},\tau) = d_{jkl}(\mathbf{x})\varepsilon_{kl}(\mathbf{x},\tau) + \alpha_{kj}(\mathbf{x})E_k(\mathbf{x},\tau) + \gamma_{jk}(\mathbf{x})H_k(\mathbf{x},\tau) + m_j(\mathbf{x})\theta(\mathbf{x},\tau), \tag{9}$$

with the strain tensor ε_{ij} being related to the displacements u_i by

$$\varepsilon_{ij} = \frac{1}{2}(u_{i,j} + u_{j,i}). \tag{10}$$

Note that the constitutive relationship for the density of entropy is omitted, since the influence of mechanical and electro-magnetic fields is neglected and the thermal problem is considered as an independent problem separately. The functional coefficients $c_{ijkl}(\mathbf{x})$, $h_{jk}(\mathbf{x})$ and $\gamma_{jk}(\mathbf{x})$ are the elastic coefficients, dielectric permittivities, and magnetic permeabilities, respectively; $e_{kij}(\mathbf{x})$, $d_{kij}(\mathbf{x})$, $\alpha_{jk}(\mathbf{x})$, $p_j(\mathbf{x})$ and $m_j(\mathbf{x})$ are the piezoelectric, piezomagnetic, magnetoelectric, pyroelectric and pyromagnetic coefficients, respectively. The stress–temperature modulus $\lambda_{ij}(\mathbf{x})$ can be expressed through the stiffness coefficients and the coefficients of linear thermal expansion β_{kl}

$$\lambda_{ij} = c_{ijkl}\beta_{kl}. \tag{11}$$

In the case of certain crystal symmetries, one can formulate also the plane-deformation problems (Parton and Kudryavtsev, 1988). For instance, in the crystals of hexagonal symmetry with x_3 being the six-order symmetry axis and assuming $u_2 = 0$ as well as the independence on x_2, i.e. $(\cdot)_{,2} = 0$, we have $\varepsilon_{22} = \varepsilon_{23} = \varepsilon_{12} = E_2 = H_2 = 0$. Then, the constitutive equations (7)–(9) are reduced to the following form:

$$\begin{bmatrix}\sigma_{11}\\ \sigma_{33}\\ \sigma_{13}\end{bmatrix} = \begin{bmatrix}c_{11} & c_{13} & 0\\ c_{13} & c_{33} & 0\\ 0 & 0 & c_{44}\end{bmatrix}\begin{bmatrix}\varepsilon_{11}\\ \varepsilon_{33}\\ 2\varepsilon_{13}\end{bmatrix} - \begin{bmatrix}0 & e_{31}\\ 0 & e_{33}\\ e_{15} & 0\end{bmatrix}\begin{bmatrix}E_1\\ E_3\end{bmatrix} - \begin{bmatrix}0 & d_{31}\\ 0 & d_{33}\\ d_{15} & 0\end{bmatrix}\begin{bmatrix}H_1\\ H_3\end{bmatrix} - \boldsymbol{\lambda}\theta = \mathbf{C}(\mathbf{x})\begin{bmatrix}\varepsilon_{11}\\ \varepsilon_{33}\\ 2\varepsilon_{13}\end{bmatrix} - \mathbf{L}(\mathbf{x})\begin{bmatrix}E_1\\ E_3\end{bmatrix} - \mathbf{K}(\mathbf{x})\begin{bmatrix}H_1\\ H_3\end{bmatrix} - \boldsymbol{\lambda}(\mathbf{x})\theta, \tag{12}$$

$$\begin{bmatrix}D_1\\ D_3\end{bmatrix} = \begin{bmatrix}0 & 0 & e_{15}\\ e_{31} & e_{33} & 0\end{bmatrix}\begin{bmatrix}\varepsilon_{11}\\ \varepsilon_{33}\\ 2\varepsilon_{13}\end{bmatrix} + \begin{bmatrix}h_{11} & 0\\ 0 & h_{33}\end{bmatrix}\begin{bmatrix}E_1\\ E_3\end{bmatrix} + \begin{bmatrix}\alpha_{11} & 0\\ 0 & \alpha_{33}\end{bmatrix}\begin{bmatrix}H_1\\ H_3\end{bmatrix} + \begin{bmatrix}p_1\\ p_2\end{bmatrix}\theta = \mathbf{G}(\mathbf{x})\begin{bmatrix}\varepsilon_{11}\\ \varepsilon_{33}\\ 2\varepsilon_{13}\end{bmatrix} + \mathbf{H}(\mathbf{x})\begin{bmatrix}E_1\\ E_3\end{bmatrix} + \mathbf{A}(\mathbf{x})\begin{bmatrix}H_1\\ H_3\end{bmatrix} + \boldsymbol{\Pi}(\mathbf{x})\theta, \tag{13}$$

$$\begin{bmatrix}B_1\\ B_3\end{bmatrix} = \begin{bmatrix}0 & 0 & d_{15}\\ d_{31} & d_{33} & 0\end{bmatrix}\begin{bmatrix}\varepsilon_{11}\\ \varepsilon_{33}\\ 2\varepsilon_{13}\end{bmatrix} + \begin{bmatrix}\alpha_{11} & 0\\ 0 & \alpha_{33}\end{bmatrix}\begin{bmatrix}E_1\\ E_3\end{bmatrix} + \begin{bmatrix}\gamma_{11} & 0\\ 0 & \gamma_{33}\end{bmatrix}\begin{bmatrix}H_1\\ H_3\end{bmatrix} + \begin{bmatrix}m_1\\ m_2\end{bmatrix}\theta = \mathbf{R}(\mathbf{x})\begin{bmatrix}\varepsilon_{11}\\ \varepsilon_{33}\\ 2\varepsilon_{13}\end{bmatrix} + \mathbf{A}(\mathbf{x})\begin{bmatrix}E_1\\ E_3\end{bmatrix} + \mathbf{F}(\mathbf{x})\begin{bmatrix}H_1\\ H_3\end{bmatrix} + \mathbf{M}(\mathbf{x})\theta, \tag{14}$$

where

$$\boldsymbol{\lambda} = \begin{bmatrix}c_{11} & c_{13} & c_{12}\\ c_{13} & c_{33} & c_{32}\\ 0 & 0 & 0\end{bmatrix}\begin{bmatrix}\beta_{11}\\ \beta_{33}\\ \beta_{22}\end{bmatrix} = \begin{bmatrix}\lambda_{11}\\ \lambda_{33}\\ 0\end{bmatrix}.$$

Recall that σ_{22} does not influence the governing equations, although it is not vanishing in general, since $\sigma_{22} = c_{12}\varepsilon_{11} + c_{23}\varepsilon_{33} - \lambda_{22}\theta$ with $\lambda_{22} = c_{12}\beta_{11} + c_{23}\beta_{33} + c_{22}\beta_{22}$.

The following essential and natural boundary conditions are assumed for the mechanical fields:

$$u_i(\mathbf{x},\tau) = \tilde{u}_i(\mathbf{x},\tau), \quad \text{on } \Gamma_u,$$
$$t_i(\mathbf{x},\tau) \equiv \sigma_{ij}n_j = \tilde{t}_i(\mathbf{x},\tau), \quad \text{on } \Gamma_t, \quad \Gamma = \Gamma_u \cup \Gamma_t.$$

For the electrical fields, we assume

$$\psi(\mathbf{x},\tau) = \tilde{\psi}(\mathbf{x},\tau), \quad \text{on } \Gamma_p,$$
$$Q(\mathbf{x},\tau) \equiv D_i(\mathbf{x},\tau)n_i(\mathbf{x}) = \widetilde{Q}(\mathbf{x},\tau), \quad \text{on } \Gamma_q, \quad \Gamma = \Gamma_p \cup \Gamma_q,$$

for the magnetic fields

$$\mu(\mathbf{x},\tau) = \tilde{\mu}(\mathbf{x},\tau), \quad \text{on } \Gamma_a,$$
$$S(\mathbf{x},\tau) \equiv B_i(\mathbf{x},\tau)n_i(\mathbf{x}) = \widetilde{S}(\mathbf{x},\tau), \quad \text{on } \Gamma_b, \quad \Gamma = \Gamma_a \cup \Gamma_b,$$

and for the thermal fields

$$\theta(\mathbf{x},\tau) = \tilde{\theta}(\mathbf{x},\tau) \quad \text{on } \Gamma_e,$$
$$q(\mathbf{x},\tau) \equiv k_{ij}\theta_{,j}(\mathbf{x},\tau)n_i(\mathbf{x}) = \tilde{q}(\mathbf{x},\tau) \quad \text{on } \Gamma_f, \quad \Gamma = \Gamma_e \cup \Gamma_f,$$

where Γ_u is the part of the global boundary Γ with prescribed displacements, while on Γ_t, Γ_p, Γ_q, Γ_a, Γ_b, Γ_e and Γ_f the traction vector, the electric potential, the normal component of the electric displacement vector, the magnetic potential and the magnetic flux, the temperature and the heat flux are prescribed, respectively. Recall that $\widetilde{Q}(\mathbf{x},\tau)$ can be considered approximately as the surface

density of free charge, provided that the permittivity of the solid is much greater than that of the surrounding medium (vacuum).

The initial conditions for the mechanical displacements are assumed as

$$u_i(\mathbf{x},\tau)|_{\tau=0} = u_i(\mathbf{x},0) \quad \text{and} \quad \dot{u}_i(\mathbf{x},\tau)|_{\tau=0} = \dot{u}_i(\mathbf{x},0) \ \text{ in } \Omega.$$

The local weak-form of the governing equation (5) can be written as (Atluri, 2004)

$$\int_{\Omega_s} \left[\sigma_{ij,j}(\mathbf{x},\tau) - \rho\ddot{u}_i(\mathbf{x},\tau) + X_i(\mathbf{x},\tau)\right] u^*_{ik}(\mathbf{x})\, d\Omega = 0, \tag{15}$$

where $u^*_{ik}(\mathbf{x})$ is a test function.

Applying the Gauss divergence theorem to the first integral one obtains

$$\int_{\partial\Omega_s} \sigma_{ij}(\mathbf{x},t) n_j(\mathbf{x}) u^*_{ik}(\mathbf{x})\, d\Gamma - \int_{\Omega_s} \sigma_{ij}(\mathbf{x},t) u^*_{ik,j}(\mathbf{x})\, d\Omega + \int_{\Omega_s} [-\rho\ddot{u}_i(\mathbf{x},t) + X_i(\mathbf{x},t)] u^*_{ik}(\mathbf{x})\, d\Omega = 0, \tag{16}$$

where $\partial\Omega_s$ is the boundary of the local subdomain which consists of three parts $\partial\Omega_s = L_s \cup \Gamma_{st} \cup \Gamma_{su}$ (Atluri, 2004). Here, L_s is the local boundary that is totally inside the global domain, Γ_{st} is the part of the local boundary which coincides with the global traction boundary, i.e., $\Gamma_{st} = \partial\Omega_s \cap \Gamma_t$, and similarly Γ_{su} is the part of the local boundary that coincides with the global displacement boundary, i.e., $\Gamma_{su} = \partial\Omega_s \cap \Gamma_u$.

By choosing a Heaviside step function as the test function $u^*_{ik}(\mathbf{x})$ in each subdomain

$$u^*_{ik}(\mathbf{x}) = \begin{cases} \delta_{ik} & \text{at } \mathbf{x} \in \Omega_s, \\ 0 & \text{at } \mathbf{x} \notin \Omega_s, \end{cases}$$

the local weak-form (16) is converted into the following local boundary-domain integral equations:

$$\int_{L_s+\Gamma_{su}} t_i(\mathbf{x},\tau)\, d\Gamma - \int_{\Omega_s} \rho\ddot{u}_i(\mathbf{x},\tau)\, d\Omega = -\int_{\Gamma_{st}} \tilde{t}_i(\mathbf{x},\tau)\, d\Gamma - \int_{\Omega_s} X_i(\mathbf{x},\tau)\, d\Omega. \tag{17}$$

Eq. (17) is recognized as the overall force equilibrium conditions on the subdomain Ω_s. Note that the local integral equation (17) is valid for both the homogeneous and nonhomogeneous solids. Nonhomogeneous material properties are included in Eq. (17) through the elastic, piezoelectric, piezomagnetic and thermo-elastic coefficients involved in the traction components

$$t_i(\mathbf{x},\tau) = \left[c_{ijkl}(\mathbf{x}) u_{k,l}(\mathbf{x},\tau) + e_{kij}(\mathbf{x})\psi_{,k}(\mathbf{x},\tau) + d_{kij}(\mathbf{x})\mu_{,k}(\mathbf{x},\tau) - \lambda_{ij}(\mathbf{x})\theta(\mathbf{x},\tau)\right] n_j(\mathbf{x}).$$

Similarly, the local weak-form of the governing equation (1) can be written as

$$\int_{\Omega_s} D_{j,j}(\mathbf{x},\tau)\, v^*(\mathbf{x})\, d\Omega = 0, \tag{18}$$

where $v^*(\mathbf{x})$ is a test function.

Applying the Gauss divergence theorem to the local weak-form (18) and choosing the Heaviside step function as the test function $v^*(\mathbf{x})$, one can obtain

$$\int_{L_s+\Gamma_{sp}} Q(\mathbf{x},\tau)\, d\Gamma = -\int_{\Gamma_{sq}} \widetilde{Q}(\mathbf{x},\tau)\, d\Gamma, \tag{19}$$

where

$$Q(\mathbf{x},\tau) = D_j(\mathbf{x},\tau) n_j(\mathbf{x}) = \left[e_{jkl} u_{k,l}(\mathbf{x},\tau) - h_{jk}\psi_{,k}(\mathbf{x},\tau) - \alpha_{jk}\mu_{,k}(\mathbf{x},\tau) + p_j\theta(\mathbf{x},\tau)\right] n_j.$$

The local integral equation corresponding to the governing equation (2) has the form

$$\int_{L_s+\Gamma_{sa}} S(\mathbf{x},\tau)\, d\Gamma = -\int_{\Gamma_{sb}} \widetilde{S}(\mathbf{x},\tau)\, d\Gamma, \tag{20}$$

where the magnetic flux is given by

$$S(\mathbf{x},\tau) = B_j(\mathbf{x},\tau) n_j(\mathbf{x}) = \left[d_{jkl} u_{k,l}(\mathbf{x},\tau) - \alpha_{kj}\psi_{,k}(\mathbf{x},\tau) - \gamma_{jk}\mu_{,k}(\mathbf{x},\tau) + m_j\theta(\mathbf{x},\tau)\right] n_j.$$

The local weak-form of the diffusion equation (6) can be written as

$$\int_{\Omega_s} \left\{ \left[k_{ij}(\mathbf{x})\theta_{,j}(\mathbf{x},\tau)\right]_{,i} - \rho(\mathbf{x}) c(\mathbf{x}) \dot{\theta}(\mathbf{x},\tau) \right\} w^*(\mathbf{x})\, d\Omega = 0, \tag{21}$$

where $w^*(\mathbf{x})$ is a test function.

Applying the Gauss divergence theorem to the local weak-form and considering the Heaviside step function for the test function $w^*(\mathbf{x})$, one can obtain

$$\int_{L_s+\Gamma_{se}} q(\mathbf{x},\tau)\, d\Gamma - \int_{\Omega_s} \rho(\mathbf{x}) c(\mathbf{x}) \dot{\theta}(\mathbf{x},\tau)\, d\Omega = -\int_{\Gamma_{sf}} \tilde{q}(\mathbf{x},\tau)\, d\Gamma. \tag{22}$$

In the MLPG method, the test and the trial functions are not necessarily from the same functional spaces. For internal nodes, the test function is chosen as a unit step function with its support on the local subdomain. The trial functions, on the other hand, are chosen to be the MLS-approximations by using a number of nodes spreading over the domain of influence. According to the MLS (Belytschko et al., 1996) method, the approximation of the displacement field can be given as

$$\mathbf{u}^h(\mathbf{x}) = \sum_{i=1}^{m} p_i(\mathbf{x}) a_i(\mathbf{x}) = \mathbf{p}^T(\mathbf{x})\mathbf{a}(\mathbf{x}),$$

where $\mathbf{p}^T(\mathbf{x}) = \{p_1(\mathbf{x}), p_2(\mathbf{x}), \ldots p_m(\mathbf{x})\}$ is a vector of complete basis functions of order m and $\mathbf{a}(\mathbf{x}) = \{a_1(\mathbf{x}), a_2(\mathbf{x}), \ldots a_m(\mathbf{x})\}$ is a vector of unknown parameters that depend on $\mathbf{x}$. For example, in 2-D problems

$$\mathbf{p}^T(\mathbf{x}) = \{1, x_1, x_3\} \quad \text{for } m = 3$$

and

$$\mathbf{p}^T(\mathbf{x}) = \{1, x_1, x_3, x_1^2, x_1x_3, x_3^2\} \quad \text{for } m = 6$$

are linear and quadratic basis functions, respectively. The basis functions are not necessary to be polynomials. It is convenient to introduce $r^{-1/2}$ – singularity for secondary fields at the crack-tip vicinity for modelling of fracture problems (Fleming et al., 1997). Then, the basis functions can be considered in the following form:

$$\mathbf{p}^T(\mathbf{x}) = \{1, x_1, x_3, \sqrt{r}\cos(\theta/2), \sqrt{r}\sin(\theta/2), \sqrt{r}\sin(\theta/2)\sin\theta, \sqrt{r}\cos(\theta/2)\sin\theta\} \quad \text{for } m = 7,$$

where r and θ are polar coordinates with the crack-tip as the origin. The upper given enriched basic functions represent all occurring terms in asymptotic expansion of displacements at the crack-tip vicinity. Then, density of node distribution in such a case can be lower than in the polynomial basis functions at the same accuracy of results.

The approximated functions for the mechanical displacements, the electric and magnetic potentials, and the temperature can be written as (Atluri, 2004)

$$\begin{aligned}
\mathbf{u}^h(\mathbf{x},\tau) &= \mathbf{\Phi}^T(\mathbf{x})\cdot\hat{\mathbf{u}} = \sum_{a=1}^{n}\phi^a(\mathbf{x})\hat{\mathbf{u}}^a(\tau),\\
\psi^h(\mathbf{x},\tau) &= \sum_{a=1}^{n}\phi^a(\mathbf{x})\hat{\psi}^a(\tau),\\
\mu^h(\mathbf{x},\tau) &= \sum_{a=1}^{n}\phi^a(\mathbf{x})\hat{\mu}^a(\tau),\\
\theta^h(\mathbf{x},\tau) &= \sum_{a=1}^{n}\phi^a(\mathbf{x})\hat{\theta}^a(\tau),
\end{aligned} \tag{23}$$

where the nodal values $\hat{\mathbf{u}}^a(\tau)=(\hat{u}_1^a(\tau),\hat{u}_3^a(\tau))^T$, $\hat{\psi}^a(\tau)$, $\hat{\mu}^a(\tau)$, and $\hat{\theta}^a(\tau)$ are fictitious parameters for the displacements, the electric and magnetic potentials and the temperature, respectively, and $\phi^a(\mathbf{x})$ is the shape function associated with the node a. The number of nodes n used for the approximation is determined by the weight function $w^a(\mathbf{x})$. A fourth-order spline-type weight function is applied in the present work

$$w^a(\mathbf{x}) = \begin{cases} 1-6\left(\frac{d^a}{r^a}\right)^2+8\left(\frac{d^a}{r^a}\right)^3-3\left(\frac{d^a}{r^a}\right)^4, & 0\leqslant d^a\leqslant r^a,\\ 0, & d^a\geqslant r^a, \end{cases} \tag{24}$$

where $d^a=\|\mathbf{x}-\mathbf{x}^a\|$ and r^a is the size of the support domain. It is seen that the C^1-continuity is ensured over the entire domain, and therefore the continuity conditions of the tractions, the electric charge, the magnetic flux and the heat flux are satisfied. In the MLS approximation, the rates of the convergence of the solution may depend upon the nodal distance as well as the size of the support domain (Wen and Aliabadi, 2007, 2008; Wen et al., 2008). It should be noted that a smaller size of the subdomains may induce larger oscillations in the nodal shape functions (Atluri, 2004). A necessary condition for a regular MLS approximation is that at least m weight functions are non-zero (i.e. $n\geqslant m$) for each sample point $\mathbf{x}\in\Omega$. This condition determines the size of the support domain.

Then, the traction vector $t_i(\mathbf{x},\tau)$ at a boundary point $\mathbf{x}\in\partial\Omega_s$ is approximated in terms of the same nodal values $\hat{\mathbf{u}}^a(\tau)$ as

$$\begin{aligned}
\mathbf{t}^h(\mathbf{x},\tau) = {}& \mathbf{N}(\mathbf{x})\mathbf{C}(\mathbf{x})\sum_{a=1}^{n}\mathbf{B}^a(\mathbf{x})\hat{\mathbf{u}}^a(\tau)+\mathbf{N}(\mathbf{x})\mathbf{L}(\mathbf{x})\sum_{a=1}^{n}\mathbf{P}^a(\mathbf{x})\hat{\psi}^a(\tau)\\
&+\mathbf{N}(\mathbf{x})\mathbf{K}(\mathbf{x})\sum_{a=1}^{n}\mathbf{P}^a(\mathbf{x})\hat{\mu}^a(\tau)-\mathbf{N}(\mathbf{x})\boldsymbol{\lambda}(\mathbf{x})\sum_{a=1}^{n}\varphi^a(\mathbf{x})\hat{\theta}^a(\tau),
\end{aligned} \tag{25}$$

where the matrices $\mathbf{C}(\mathbf{x})$, $\mathbf{L}(\mathbf{x})$ and $\mathbf{K}(\mathbf{x})$ are defined in Eq. (12), the matrix $\mathbf{N}(\mathbf{x})$ is related to the normal vector $\mathbf{n}(\mathbf{x})$ on $\partial\Omega_s$ by

$$\mathbf{N}(\mathbf{x}) = \begin{bmatrix} n_1 & 0 & n_3\\ 0 & n_3 & n_1 \end{bmatrix},$$

and finally, the matrices $\mathbf{B}^a$ and $\mathbf{P}^a$ are represented by the gradients of the shape functions as

$$\mathbf{B}^a(\mathbf{x}) = \begin{bmatrix} \phi^a_{,1} & 0\\ 0 & \phi^a_{,3}\\ \phi^a_{,3} & \phi^a_{,1} \end{bmatrix}, \quad \mathbf{P}^a(\mathbf{x}) = \begin{bmatrix} \phi^a_{,1}\\ \phi^a_{,3} \end{bmatrix}.$$

Similarly the normal component of the electric displacement vector $Q(\mathbf{x},\tau)$ can be approximated by

$$\begin{aligned}
Q^h(\mathbf{x},\tau) = {}& \mathbf{N}_1(\mathbf{x})\mathbf{G}(\mathbf{x})\sum_{a=1}^{n}\mathbf{B}^a(\mathbf{x})\hat{\mathbf{u}}^a(\tau)-\mathbf{N}_1(\mathbf{x})\mathbf{H}(\mathbf{x})\sum_{a=1}^{n}\mathbf{P}^a(\mathbf{x})\hat{\psi}^a(\tau)\\
&-\mathbf{N}_1(\mathbf{x})\mathbf{A}(\mathbf{x})\sum_{a=1}^{n}\mathbf{P}^a(\mathbf{x})\hat{\mu}^a(\tau)+\mathbf{N}_1(\mathbf{x})\mathbf{\Pi}(\mathbf{x})\sum_{a=1}^{n}\phi^a(\mathbf{x})\hat{\theta}^a(\tau),
\end{aligned} \tag{26}$$

where the matrices $\mathbf{G}(\mathbf{x})$, $\mathbf{H}(\mathbf{x})$, $\mathbf{\Pi}(\mathbf{x})$ and $\mathbf{A}(\mathbf{x})$ are defined in Eq. (13) and

$$\mathbf{N}_1(\mathbf{x}) = [\,n_1 \quad n_3\,].$$

Eventually, the magnetic flux $S(\mathbf{x},\tau)$ is approximated by

$$\begin{aligned}
S^h(\mathbf{x},\tau) = {}& \mathbf{N}_1(\mathbf{x})\mathbf{R}(\mathbf{x})\sum_{a=1}^{n}\mathbf{B}^a(\mathbf{x})\hat{\mathbf{u}}^a(\tau)-\mathbf{N}_1(\mathbf{x})\mathbf{A}(\mathbf{x})\\
&\times\sum_{a=1}^{n}\mathbf{P}^a(\mathbf{x})\hat{\psi}^a(\tau)-\mathbf{N}_1(\mathbf{x})\mathbf{F}(\mathbf{x})\sum_{a=1}^{n}\mathbf{P}^a(\mathbf{x})\hat{\mu}^a(\tau)\\
&+\mathbf{N}_1(\mathbf{x})\mathbf{M}(\mathbf{x})\sum_{a=1}^{n}\phi^a(\mathbf{x})\hat{\theta}^a(\tau)
\end{aligned} \tag{27}$$

with the matrices $\mathbf{R}(\mathbf{x})$, $\mathbf{F}(\mathbf{x})$ and $\mathbf{M}(\mathbf{x})$ being defined in Eq. (14).

The heat flux $q(\mathbf{x},\tau)$ is approximated by

$$q^h(\mathbf{x},\tau) = k_{ij}n_i\sum_{a=1}^{n}\phi^a_{,j}(\mathbf{x})\hat{\theta}^a(\tau) = \mathbf{N}_1(\mathbf{x})\mathbf{\Theta}(\mathbf{x})\sum_{a=1}^{n}\mathbf{P}^a(\mathbf{x})\hat{\theta}^a(\tau), \tag{28}$$

where $\mathbf{\Theta}(\mathbf{x}) = \begin{bmatrix} k_{11} & k_{13}\\ k_{13} & k_{33} \end{bmatrix}$.

Satisfying the essential boundary conditions and making use of the approximation formulae (23), one obtains the discretized form of these boundary conditions as

$$\begin{aligned}
&\sum_{a=1}^{n}\phi^a(\zeta)\hat{\mathbf{u}}^a(\tau) = \tilde{\mathbf{u}}(\zeta,\tau) \quad \text{for } \zeta\in\Gamma_u,\\
&\sum_{a=1}^{n}\phi^a(\zeta)\hat{\psi}^a(\tau) = \tilde{\psi}(\zeta,\tau) \quad \text{for } \zeta\in\Gamma_p,\\
&\sum_{a=1}^{n}\phi^a(\zeta)\hat{\mu}^a(\tau) = \tilde{\mu}(\zeta,\tau) \quad \text{for } \zeta\in\Gamma_a,\\
&\sum_{a=1}^{n}\phi^a(\zeta)\hat{\theta}^a(\tau) = \tilde{\theta}(\zeta,\tau) \quad \text{for } \zeta\in\Gamma_e.
\end{aligned} \tag{29}$$

Furthermore, in view of the MLS-approximations (25)–(28) for the unknown quantities in the local boundary-domain integral equations (17), (19), (20) and (22), we obtain their discretized forms as

$$\begin{aligned}
&\sum_{a=1}^{n}\left[\left(\int_{L_s+\Gamma_{st}}\mathbf{N}(\mathbf{x})\mathbf{C}(\mathbf{x})\mathbf{B}^a(\mathbf{x})\,d\Gamma\right)\hat{\mathbf{u}}^a(\tau)-\left(\int_{\Omega_s}\rho(\mathbf{x})\phi^a\,d\Omega\right)\ddot{\hat{\mathbf{u}}}^a(\tau)\right]\\
&+\sum_{a=1}^{n}\left(\int_{L_s+\Gamma_{st}}\mathbf{N}(\mathbf{x})\mathbf{L}(\mathbf{x})\mathbf{P}^a(\mathbf{x})\,d\Gamma\right)\hat{\psi}^a(\tau)\\
&+\sum_{a=1}^{n}\left(\int_{L_s+\Gamma_{st}}\mathbf{N}(\mathbf{x})\mathbf{K}(\mathbf{x})\mathbf{P}^a(\mathbf{x})\,d\Gamma\right)\hat{\mu}^a(\tau)\\
&-\sum_{a=1}^{n}\left(\int_{L_s+\Gamma_{st}}\mathbf{N}(\mathbf{x})\boldsymbol{\lambda}(\mathbf{x})\phi^a(\mathbf{x})\,d\Gamma\right)\hat{\theta}^a(\tau)\\
&=-\int_{\Gamma_{st}}\tilde{\mathbf{t}}(\mathbf{x},\tau)\,d\Gamma-\int_{\Omega_s}\mathbf{X}(\mathbf{x},\tau)\,d\Omega,
\end{aligned} \tag{30}$$

$$\begin{aligned}
&\sum_{a=1}^{n}\left(\int_{L_s+\Gamma_{sq}}\mathbf{N}_1(\mathbf{x})\mathbf{G}(\mathbf{x})\mathbf{B}^a(\mathbf{x})\,d\Gamma\right)\hat{\mathbf{u}}^a(\tau)\\
&-\sum_{a=1}^{n}\left(\int_{L_s+\Gamma_{sq}}\mathbf{N}_1(\mathbf{x})\mathbf{H}(\mathbf{x})\mathbf{P}^a(\mathbf{x})\,d\Gamma\right)\hat{\psi}^a(\tau)\\
&-\sum_{a=1}^{n}\left(\int_{L_s+\Gamma_{sq}}\mathbf{N}_1(\mathbf{x})\mathbf{A}(\mathbf{x})\mathbf{P}^a(\mathbf{x})\,d\Gamma\right)\hat{\mu}^a(\tau)\\
&+\sum_{a=1}^{n}\left(\int_{L_s+\Gamma_{sq}}\mathbf{N}_1(\mathbf{x})\mathbf{\Pi}(\mathbf{x})\phi^a(\mathbf{x})\,d\Gamma\right)\hat{\theta}^a(\tau)\\
&=-\int_{\Gamma_{sq}}\tilde{Q}(\mathbf{x},\tau)\,d\Gamma,
\end{aligned} \tag{31}$$

$$\sum_{a=1}^{n}\left(\int_{L_s+\Gamma_{sb}}\mathbf{N}_1(\mathbf{x})\mathbf{R}(\mathbf{x})\mathbf{B}^a(\mathbf{x})\,d\Gamma\right)\hat{\mathbf{u}}^a(\tau)-\sum_{a=1}^{n}\left(\int_{L_s+\Gamma_{sb}}\mathbf{N}_1(\mathbf{x})\mathbf{A}(\mathbf{x})\mathbf{P}^a(\mathbf{x})\,d\Gamma\right)\hat{\boldsymbol{\psi}}^a(\tau)-\sum_{a=1}^{n}\left(\int_{L_s+\Gamma_{sb}}\mathbf{N}_1(\mathbf{x})\mathbf{F}(\mathbf{x})\mathbf{P}^a(\mathbf{x})\,d\Gamma\right)\hat{\boldsymbol{\mu}}^a(\tau)+\sum_{a=1}^{n}\left(\int_{L_s+\Gamma_{sb}}\mathbf{N}_1(\mathbf{x})\mathbf{M}(\mathbf{x})\phi^a(\mathbf{x})\,d\Gamma\right)\hat{\theta}^a(\tau)=-\int_{\Gamma_{sb}}\widetilde{S}(\mathbf{x},\tau)\,d\Gamma, \tag{32}$$

$$\sum_{a=1}^{n}\left[\left(\int_{L_s+\Gamma_{sf}}\mathbf{N}_1(\mathbf{x})\boldsymbol{\Theta}(\mathbf{x})\mathbf{P}^a(\mathbf{x})\,d\Gamma\right)\hat{\theta}^a(\tau)-\left(\int_{\Omega_s}\rho c\phi^a(\mathbf{x})\,d\Gamma\right)\dot{\hat{\theta}}^a(\tau)\right]=-\int_{\Gamma_{sf}}\tilde{q}(\mathbf{x},\tau)\,d\Gamma, \tag{33}$$

which are considered on the sub-domains adjacent to the interior nodes as well as to the boundary nodes on Γ_{st}, Γ_{sq} and Γ_{sb}.

Collecting the discretized local boundary-domain integral equations together with the discretized boundary conditions for the displacements, the electrical and magnetic potentials, and the temperature results in a complete system of ordinary differential equations and it can be rearranged in such a way that all known quantities are on the right-hand side. Thus, in matrix form the system becomes

$$\mathbf{A}\ddot{\mathbf{x}}+\mathbf{B}\dot{\mathbf{x}}+\mathbf{C}\mathbf{x}=\mathbf{Y}. \tag{34}$$

Recall that the system matrix has a block structure and the thermal unknowns can be solved separately from the mechanical and electro-magnetic unknowns.

There are many time integration procedures for the solution of this system of ordinary differential equations. In the present work, the Houbolt method is applied. In the Houbolt finite-difference scheme (Houbolt, 1950), the "acceleration" ($\ddot{\mathbf{u}}=\ddot{\mathbf{x}}$) is expressed as

$$\ddot{\mathbf{x}}_{\tau+\Delta\tau}=\frac{2\mathbf{x}_{\tau+\Delta\tau}-5\mathbf{x}_{\tau}+4\mathbf{x}_{\tau-\Delta\tau}-\mathbf{x}_{\tau-2\Delta\tau}}{\Delta\tau^2}, \tag{35}$$

where $\Delta\tau$ is the time step. The backward difference method is applied for the approximation of "velocities"

$$\dot{\mathbf{x}}_{\tau+\Delta\tau}=\frac{\mathbf{x}_{\tau+\Delta\tau}-\mathbf{x}_{\tau}}{\Delta\tau}. \tag{36}$$

Substituting Eqs. (35) and (36) into Eq. (34), we get the following system of algebraic equations for the unknowns $\mathbf{x}_{\tau+\Delta\tau}$:

$$\left[\frac{2}{\Delta\tau^2}\mathbf{A}+\frac{1}{\Delta\tau}\mathbf{B}+\mathbf{C}\right]\mathbf{x}_{\tau+\Delta\tau}=\frac{1}{\Delta\tau^2}(5\mathbf{A}+\mathbf{B}\Delta\tau)\mathbf{x}_{\tau}+\mathbf{A}\frac{1}{\Delta\tau^2}\{-4\mathbf{x}_{\tau-\Delta\tau}+\mathbf{x}_{\tau-2\Delta\tau}\}+\mathbf{Y}. \tag{37}$$

The value of the time step has to be appropriately selected with respect to material parameters (wave velocities) and time dependence of the boundary conditions.

3. Numerical examples

In all numerical examples presented in this section, impermeable crack-face boundary conditions for electrical and magnetic fields are assumed.

3.1. A central crack in a finite homogeneous strip

In the first example, a straight central crack in a finite strip under a thermal load is analyzed. The geometry of the strip is given in Fig. 1 with the following values: $a=0.5$, $a/w=0.4$ and $h/w=1.2$. On the outer boundary of the strip a thermal load $T_2=\theta_0=1^\circ$ is applied. On both crack surfaces vanishing value of temperature is kept. The outer boundary is free of traction, electrical displacement and magnetic induction.

Due to the symmetry of the problem with respect to both Cartesian coordinates, only a quarter of the strip is modeled. We have used 930 (31×30) nodes equidistantly distributed for the MLS approximation of the physical quantities (Fig. 2). The local subdomains are considered to be circular with a radius $r_{loc}=0.025$ m. Homogeneous material properties are selected to test the present

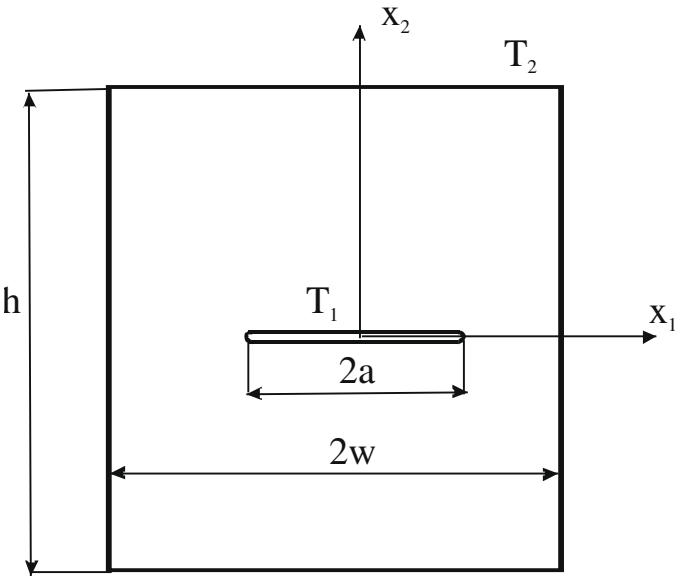

Fig. 1. Central crack in a finite strip with prescribed temperatures on outer boundary and crack surfaces.

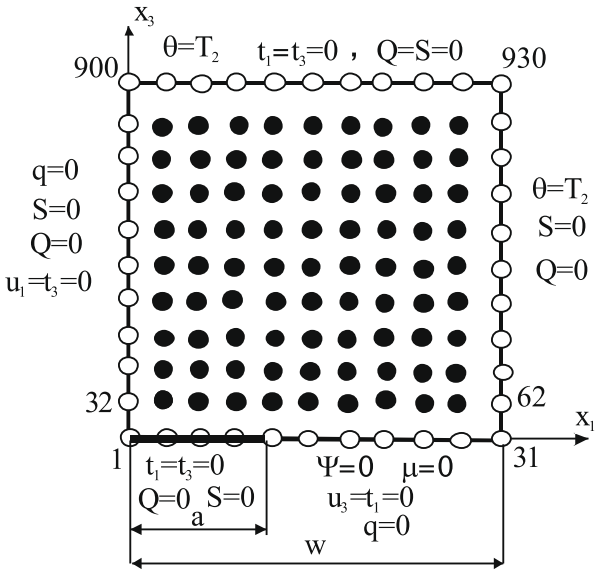

Fig. 2. Node distribution and boundary conditions.

computational method. The material coefficients for the $BaTiO_3$–$CoFe_2O_4$ composite are given by Ootao and Tanigawa (2005) as

$c_{11} = 22.6 \times 10^{10}$ N m^{-2}, $c_{13} = 12.4 \times 10^{10}$ N m^{-2},
$c_{33} = 21.6 \times 10^{10}$ N m^{-2}, $c_{66} = 4.4 \times 10^{10}$ N m^{-2},

$e_{15} = 5.8$ C m^{-2}, $e_{31} = -2.2$ C m^{-2}, $e_{33} = 9.3$ C m^{-2},

$h_{11} = 5.64 \times 10^{-9}$ C^2/N m^2, $h_{33} = 6.35 \times 10^{-9}$ C^2/N m^2,

$d_{15} = 275.0$ N/A m, $d_{21} = 290.2$ N/A m, $d_{22} = 350.0$ N/A m,

$\alpha_{11} = 5.367 \times 10^{-12}$N s/V C, $\alpha_{33} = 2737.5 \times 10^{-12}$N s/V C,

$\gamma_{11} = 297.0 \times 10^{-6}$ N s^2 C^{-2}, $\gamma_{33} = 83.5 \times 10^{-6}$ N s^2 C^{-2},
$\rho = 5500$ kg/m^3,

$k_{11} = 50$ W/K m, $k_{33} = 75$ W/K m, $\beta_{11} = 0.88 \times 10^{-5}$ 1/K,
$\beta_{33} = \beta_{22} = 0.5 \times 10^{-5}$ 1/K,

$p_1 = 0$, $p_3 = -1 \times 10^{-4}$ C/K m^2, $c = 420$ W s kg^{-1} K^{-1},

$m_1 = 0$, $m_3 = -1.1 \times 10^{-4}$ N/A m K.

The crack-opening-displacements, the electrical and magnetic potentials for vanishing and finite values of pyroelectric and pyromagnetic parameters are mutually compared in Figs. 3–5. The considered finite values of the pyroelectric and pyromagnetic parameters reduce the crack-opening-displacements. Oppositely, the electrical potential is significantly increased if finite values of pyroelectric and pyromagnetic parameters are considered (Fig. 4). The magnetic potential is slightly reduced for finite values of the pyroelectric and pyromagnetic parameters (Fig. 5).

For cracks in homogeneous and linear piezoelectric and piezomagnetic solids, the asymptotic behaviour of the field quantities has been given by Wang and Mai (2003). In the crack-tip vicinity, the displacements and potentials show the classical $\sqrt{r}$ asymptotic behaviour. Hence, correspondingly, the stresses, electrical displacement and magnetic induction exhibit $1/\sqrt{r}$ behaviour, where r is the radial polar coordinate with origin at the crack-tip.

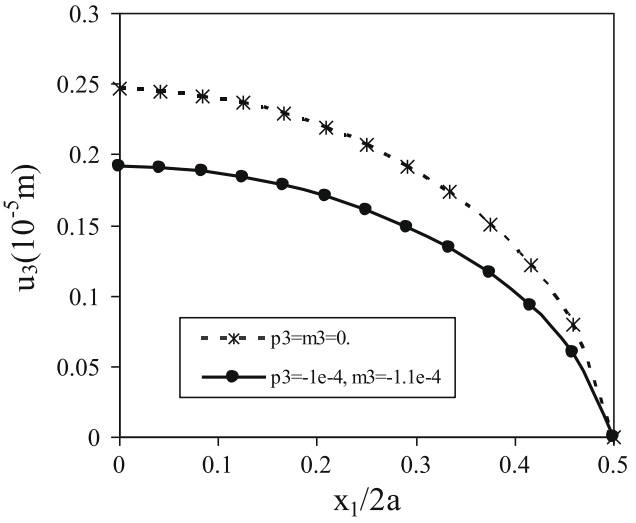

Fig. 3. Variations of the crack-opening-displacement with the normalized coordinate $x_1/2a$.

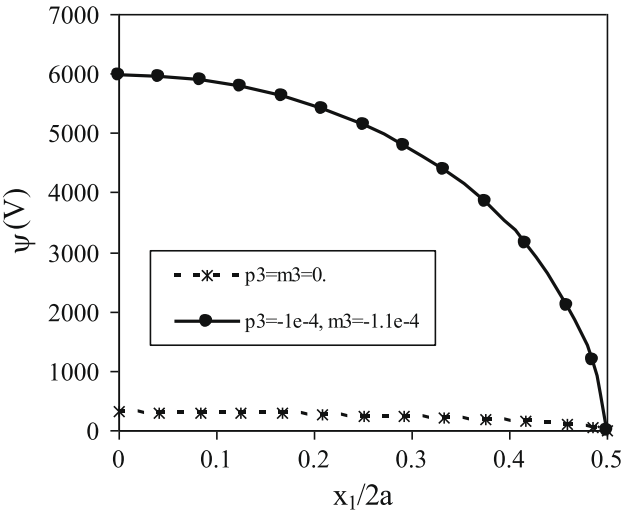

Fig. 4. Variations of the electrical potential along the crack face.

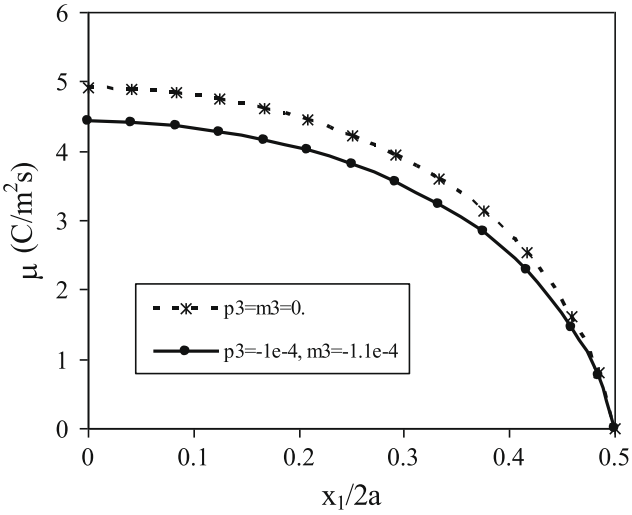

Fig. 5. Variations of the magnetic potential along the crack face.

Garcia-Sanchez et al. (2007a,b) extended the approach used in piezoelectricity to magnetoelectroelasticity to obtain asymptotic expressions of generalized intensity factors as

$$\begin{pmatrix} K_{\mathrm{II}} \\ K_{\mathrm{I}} \\ K_{\mathrm{E}} \\ K_{\mathrm{M}} \end{pmatrix} = \sqrt{\frac{\pi}{2r}} \left[Re(\mathbf{B})^{-1} \right] \begin{pmatrix} u_1 \\ u_3 \\ \psi \\ \mu \end{pmatrix}, \tag{38}$$

where the matrix **B** is determined by the material properties (Garcia-Sanchez et al., 2005, 2007b) and

$$K_{\mathrm{I}} = \lim_{r \to 0} \sqrt{2\pi r}\sigma_{33}(r,0),$$
$$K_{\mathrm{II}} = \lim_{r \to 0} \sqrt{2\pi r}\sigma_{13}(r,0),$$
$$K_{\mathrm{E}} = \lim_{r \to 0} \sqrt{2\pi r}D_3(r,0),$$
$$K_{\mathrm{M}} = \lim_{r \to 0} \sqrt{2\pi r}B_3(r,0),$$

are the stress intensity factors (SIFs) K_{I} and K_{II}, the electrical displacement intensity factor (EDIF) K_{E}, and is the magnetic induction intensity factor (MIIF) K_{M}, respectively.

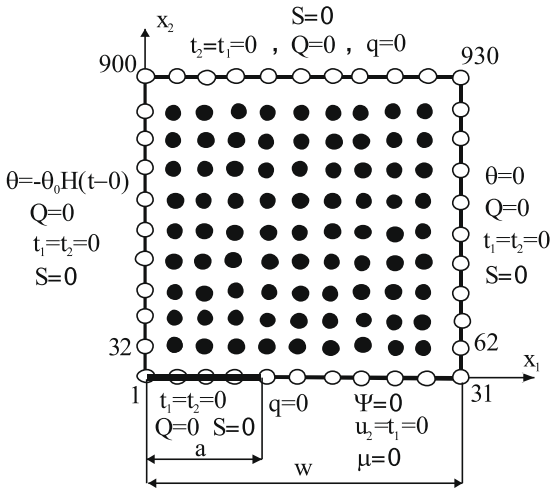

Fig. 6. Edge crack in a finite strip under a thermal shock on the lateral side.

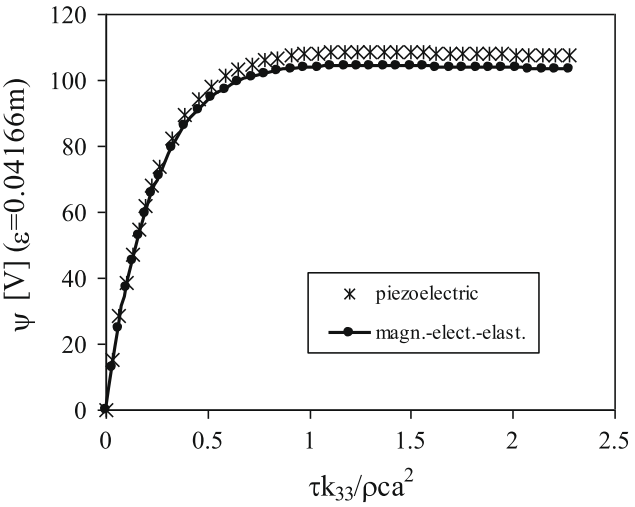

Fig. 8. Time evolution of the electrical potential at the crack-tip vicinity.

The finite values of pyroelectric and pyromagnetic parameters have vanishing influence on the stress intensity factor and its vale is $K_I = 4.48 \times 10^5$ Pa m$^{1/2}$. This value has been computed from Eq. (38) by extrapolation to the crack-tip from quantities (u_1, u_3, ψ, μ) at selected distances r from the crack-tip. Recently, Sladek et al. (2007a) have showed that electrical potential ψ caused by a remote pure mechanical load is identical to u_3 caused by a remote pure electric displacement loading as a consequence of the extended Betti's reciprocal theorem in stationary piezoelasticity. The Betti's reciprocal theorem has to valid also in stationary electro-magneto-elasticity. It is interesting to note that for a pure mechanical load, a finite values of the electrical and magnetic potentials ψ, μ on crack surfaces do not result in a finite value of the EDIF, K_E and the MIIF, K_M. It means that the crack-opening-displacement u_3 and the potentials ψ, μ are coupled, but the SIF, and the EDIF and MIIF in this case are uncoupled.

3.2. Edge crack in a finite strip under a thermal shock

Next, an edge crack in a finite magneto-electro-elastic strip is analyzed. On the left lateral side of the strip a cooling shock with Heaviside time variation is applied. The right lateral side is kept at vanishing temperature. The heat flux is vanishing on the top of the strip. The geometry of the strip is given in Fig. 6 with the following values: $a = 0.5$, $a/w = 0.4$ and $h/w = 1.2$. Due to the symmetry of the problem with respect to the x_1-axis, only a half of the strip is modeled. We have used 930 nodes equidistantly distributed for the MLS approximation of the physical quantities. The material properties are the same as in the previous example. Numerical calculations are carried out for a time step $\Delta\tau = 250$ s.

The time evolutions of the displacement and the electrical potential at a small distance $\varepsilon = 0.04166$ m from the crack-tip are presented in Figs. 7 and 8, respectively. One can see that the considered electromagnetic and piezomagnetic parameters have only small influence on the displacement and electrical potential. For a piezoelectric material both electromagnetic and piezomagnetic parameters are zero.

Variations of the displacement, electrical and magnetic potentials along the crack face at the time instant $\tau^* = 0.909$ are presented in Fig. 9. These quantities are used for evaluation of the intensity factors from Eq. (38). One can observe that the gradient of the crack-opening-displacement along x_1 is significantly larger than in the previous central crack problem.

Numerical results for the normalized stress intensity factor $f_I = K_I/(\sqrt{\pi a}\beta_{11}c_{11}\theta_0)$ are presented in Fig. 10. The time evolution of the SIF is similar to the variation of displacements at the

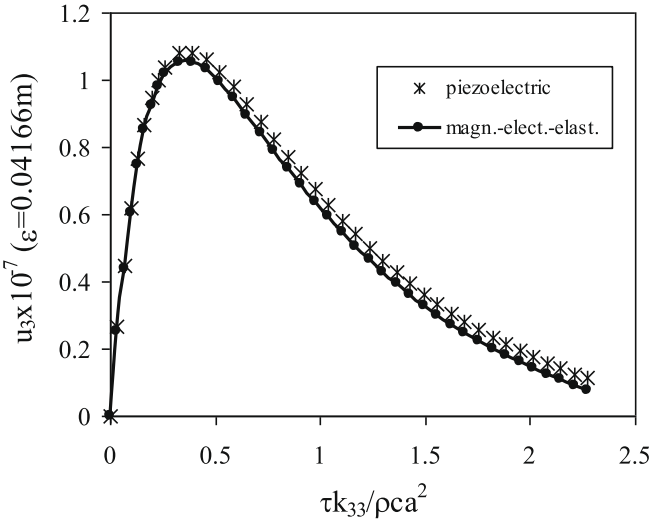

Fig. 7. Time evolution of the crack displacement at the crack-tip vicinity.

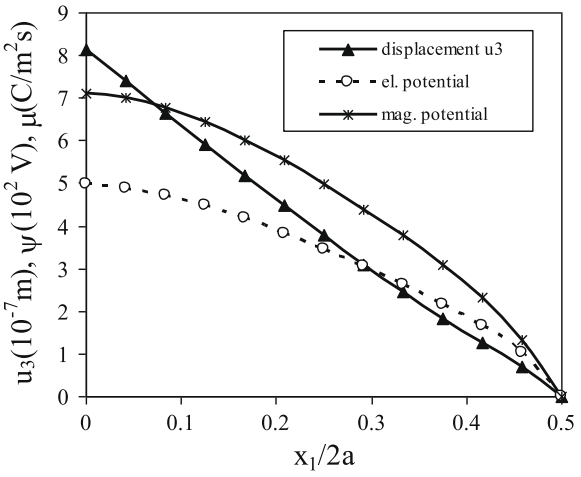

Fig. 9. Variations of the displacement, electrical and magnetic potentials along the crack face at $\tau^* = 0.909$.

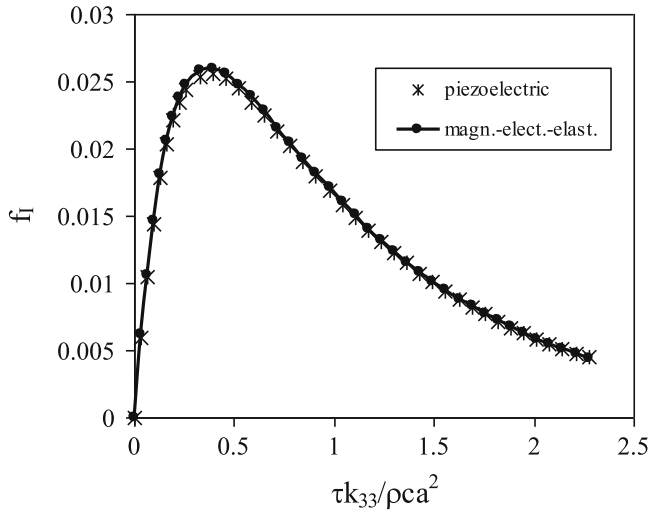

Fig. 10. Time evolution of the normalized SIF in the cracked strip under a thermal shock.

crack-tip vicinity presented in Fig. 7. It means that displacements have dominant influence on the value of the SIF for considered material parameters. One can observe that for a large instant the SIF is approaching the stationary value $f_{\mathrm{I}}^{\mathrm{stat}} = 0.00002$. Stationary value of the SIF gives a test of accuracy, since this value should be vanishing due to vanishing stresses ahead the crack-tip for considered boundary conditions. The EDIF for considered boundary value problem should be vanishing too (Fig. 11). The normalized EDIF is defined as $f_{IV} = \Lambda K_{\mathrm{E}}/(\sqrt{\pi a}\beta_{11}c_{11}\theta_0)$, where $\Lambda = e_{33}/h_{33}$. Due to the extended Betti's reciprocal theorem the potential ψ on the crack caused by a remote pure mechanical load is identical to the displacement u_3 caused by a remote pure electric displacement loading (Sladek et al., 2007b). Therefore, for a pure mechanical loading, a finite value of the potential ψ on the crack does not result in a finite value of the EDIF K_{E}. It means that the crack-opening-displacement u_3 and the potential are coupled, but the SIF and the EDIF in this case are uncoupled.

The influence of the material gradation on the stress intensity factor is analyzed too. The functionally graded material properties in the x_1-direction are considered. The gradation of material properties in the strip is illustrated in Fig. 12. An exponential variation of the elastic, piezoelectric, dielectric, paramagnetic, electromagnetic and magnetic permeability coefficients is assumed as

$$f_{ij}(\mathbf{x}) = f_{ij0}\exp(\gamma_f x_1), \tag{39}$$

where the symbol f_{ij} is commonly used for particular material coefficients with f_{ij0} corresponding to the material coefficients for the $BaTiO_3$–$CoFe_2O_4$. We have considered the same exponential gradation for all coefficients with value $\gamma = 1$ in the numerical calculations. Then, all mechanical, electrical and magnetic parameters at the crack-tip are $e^{0.5} = 1.649$ times larger than that in the homogeneous material. The heat conduction and linear thermal expansion coefficients have negative gradation coefficient $\gamma = -1$. It means that both thermal coefficients are decreasing along x_1. Pyroelectric and pyromagnetic coefficients are assumed to be zero in our case. Again the time step $\Delta\tau = 250$ s is considered in numerical analysis.

Larger stiffness parameters have a tendency to decrease the displacements. The equivalent thermal forces are the same for the FGM and homogeneous material since increasing stiffness and deceasing thermal expansion are mutually eliminated. If we consider an imaginary homogeneous material characterized by the material parameters corresponding to that of the FGM with $\gamma = 1$ at the crack-tip $x_1 = 0.5$, the crack-opening-displacement and potentials are significantly reduced in comparison with ones corresponding to the real homogeneous material with parameters f_{ij0}. However, the SIF is the same for both imaginary and real homogeneous materials. Due to lower stiffness parameters for $x_1 < 0.5$ in the FGM, the crack-opening-displacements and potentials are larger in FGM than in the imaginary homogeneous material. From the numerical analyses it follows that the crack-opening-displacement and potential values are similar in the real homogeneous and continuously nonhomogeneous material for considered material parameters. However, the elastic, piezoelectric, dielectric, paramagnetic, electromagnetic and magnetic permeability coefficients at the crack-tip are 1.649 times larger than that in the homogeneous case. Then, it follows from Eq. (38) that the SIF is larger for FGM material under a thermal load than in the homogeneous one.

The time evolution of the SIF in the cracked strip under a cooling shock is presented in Fig. 13. The normalized stationary SIF for the considered load and geometry is equal to $f_{\mathrm{I}}^{\mathrm{stat}} = 0.0176$. One can observe that SIF is approaching its stationary value at a large time. Since the thermal conductivity is smaller than that in the homogeneous case, the peak value of the SIF is reached at larger time for FGM.

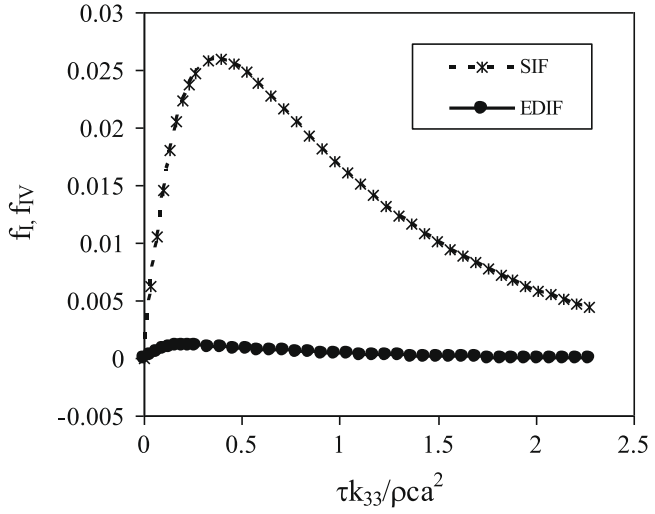

Fig. 11. Comparison of the normalized SIF and EDIF in the cracked strip under a thermal shock.

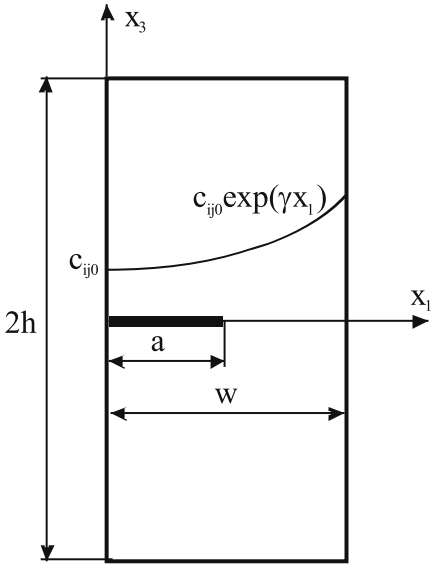

Fig. 12. An edge crack in a finite strip with graded material properties in x_1.

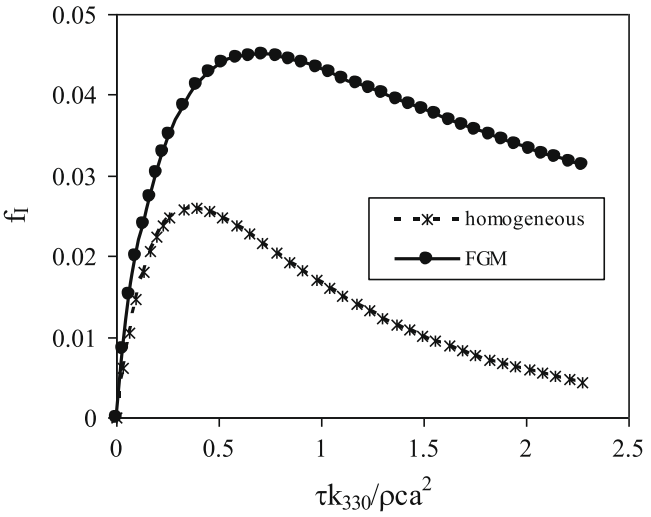

Fig. 13. Time evolution of the SIF in the cracked FGM strip under a thermal shock.

4. Conclusions

A meshless local Petrov–Galerkin method (MLPG) is presented for 2-D crack problems in continuously nonhomogeneous magneto-electro-thermo-elastic solids subjected to thermal loadings. Stationary and transient thermal conditions are considered in the heat conduction equation. Also the inertial term is considered in the equations of motion. The coupled governing partial differential equations are satisfied in a weak-form on small fictitious subdomains. A unit step function is used as the test function in the local weak-form of the governing partial differential equations on small circular subdomains spread on the analyzed domain. The moving least-squares (MLS) scheme is adopted for the approximation of the physical field quantities. One obtains a system of ordinary differential equations for certain nodal unknowns. That system is solved numerically by the Houbolt finite-difference scheme. The proposed method is a truly meshless method, which requires neither domain elements nor background cells in either the interpolation or the integration.

The present method is an alternative numerical tool to many existing computational methods such as the FEM or the BEM. The main advantage of the present method is its simplicity. Compared to the conventional BEM, the present method requires no fundamental solutions and all integrands in the present formulation are regular. Thus, no special numerical techniques are required to evaluate the integrals. It should be noted here that the fundamental solutions are not available for magneto-electro-elastic solids with continuously varying material properties in general cases. The present formulation also possesses the generality of the FEM. Therefore, the method is promising for numerical analysis of multi-field problems like piezoelectric, electro-magnetic or thermoelastic problems, which cannot be solved efficiently by the conventional BEM.

Acknowledgements

The authors acknowledge the support by the Slovak Science and Technology Assistance Agency registered under number APVV-0427-07, the Slovak Grant Agency VEGA-2/0039/09, and the German Research Foundation (DFG, Project No. ZH 15/14-1).

References

Alshits, V.I., Darinski, A.N., Lothe, J., 1992. On the existence of surface waves in half-anisotropic elastic media with piezoelectric and piezomagnetic properties. Wave Motion 16, 265–283.

Atluri, S.N., 2004. The Meshless Method, (MLPG) for Domain & BIE Discretizations. Tech Science Press.

Atluri, S.N., Sladek, J., Sladek, V., Zhu, T., 2000. The local boundary integral equation (LBIE) and its meshless implementation for linear elasticity. Computational Mechanics 25, 180–198.

Atluri, S.N., Han, Z.D., Shen, S., 2003. Meshless local Petrov–Galerkin (MLPG) approaches for solving the weakly-singular traction & displacement boundary integral equations. CMES: Computer Modeling in Engineering & Sciences 4, 507–516.

Avellaneda, M., Harshe, G., 1994. Magnetoelectric effect in piezoelectric/magnetostrictive multilayer (2–2) composites. Journal of Intelligent Material Systems and Structures 5, 501–513.

Belytschko, T., Krogauz, Y., Organ, D., Fleming, M., Krysl, P., 1996. Meshless methods: an overview and recent developments. Computer Methods in Applied Mechanics and Engineering 139, 3–47.

Beom, H.G., Atluri, S.N., 2003. Effect of electric fields on fracture behavior of ferroelectric ceramics. Journal of Mechanics and Physics of Solids 51, 1107–1125.

Berlingcourt, D.A., Curran, D.R., Jaffe, H., 1964. Piezoelectric and piezomagnetic materials and their function in transducers. Physical Acoustics 1, 169–270.

Chung, M.Y., Ting, T.C.T., 1995. The Green function for a piezoelectric piezomagnetic anisotropic elastic medium with an elliptic hole or rigid inclusion. Philosophical Magazine Letters 72, 405–410.

Drobenko, B., Hachkevych, O., Kournytskyi, T., 2008. Thermomechanical behavior of polariable and magnetizable electroconductive solids subjected to induction heating. Journal of Engineering Mathematics 61, 249–269.

Eringen, C.E., Maugin, M.A., 1990. Electrodynamics of Continua. Springer, Berlin.

Feng, W.J., Su, R.K.L., 2006. Dynamic internal crack problem of a functionally graded magneto-electro-elastic strip. International Journal Solids and Structures 43, 5196–5216.

Fleming, M., Chu, Y.A., Moran, B., Belytschko, T., 1997. Enriched element-free Galerkin methods for crack-tip fields. International Journal for Numerical Methods in Engineering 40, 1483–1504.

Gao, C.F., Kessler, H., Balke, H., 2003. Crack problems in magnetoelectroelastic solids. Part I: exact solution of a crack. International Journal of Engineering Science 41, 969–981.

Garcia-Sanchez, F., Saez, A., Dominguez, J., 2005. Anisotropic and piezoelectric materials fracture analysis by BEM. Computers & Structures 83, 804–820.

Garcia-Sanchez, F., Zhang, Ch., Sladek, J., Sladek, V., 2007a. 2-D transient dynamic crack analysis in piezoelectric solids by BEM. Computational Materials Science 39, 179–186.

Garcia-Sanchez, F., Rojas-Diaz, R., Saez, A., Zhang, Ch., 2007b. Fracture of magnetoelectroelastic composite materials using boundary element method (BEM). Theoretical and Applied Fracture Mechanics 47, 192–204.

Han, F., Pan, E., Roy, A.K., Yue, Z.Q., 2006. Responses of piezoelectric, transversally isotropic, functionally graded and multilayered half spaces to uniform circular surface loading. CMES: Computer Modeling in Engineering & Sciences 14, 15–30.

He, T.H., Li, S.R., 2006. A two-dimensional generalized electromagneto-thermoelastic problem for a half-space. Journal of Thermal Stresses 29, 683–698.

Houbolt, J.C., 1950. A recurrence matrix solution for the dynamic response of elastic aircraft. Journal of Aeronautical Sciences 17, 371–376.

Huang, J.H., Kuo, W.S., 1997. The analysis of piezoelectric/piezomagnetic composite materials containing ellipsoidal inclusions. Journal of Applied Physics 81, 1378–1386.

Hu, K.Q., Li, G.Q., Zhong, Z., 2006. Fracture of a rectangular piezoelectromagnetic body. Mechanics Research Communication 33, 482–492.

Landau, L.D., Lifshitz, E.M., 1984. In: Lifshitz, E.M., Pitaevskii, L.P. (Eds.), Electrodynamics of Continuous Media, second ed. Pergamon Press, New York.

Li, J.Y., 2000. Magnetoelectroelastic multi-inclusion and inhomogeneity problems and their applications in composite materials. International Journal of Engineering Science 38, 1993–2011.

Liu, J.X., Liu, X.L., Zhao, Y.B., 2001. Green's functions for anisotropic magnetoelectroelastic solids with an elliptical cavity or a crack. International Journal of Engineering Sciences 39, 1405–1418.

Liu, G.R., Dai, K.Y., Lim, K.M., Gu, Y.T., 2002. A point interpolation mesh free method for static and frequency analysis of two-dimensional piezoelectric structures. Computational Mechanics 29, 510–519.

Mindlin, R.D., 1974. Equations of high frequency vibrations of thermopiezoelasticity problems. International Journal of Solids and Structures 10, 625–637.

Nan, C.W., 1994. Magnetoelectric effect in composites of piezoelectric and piezomagnetic phases. Physical Review B 50, 6082–6088.

Nowacki, W., 1978. Some general theorems of thermo-piezoelectricity. Journal of Thermal Stresses 1, 171–182.

Ohs, R.R., Aluru, N.R., 2001. Meshless analysis of piezoelectric devices. Computational Mechanics 27, 23–36.

Ootao, Y., Tanigawa, Y., 2005. Transient analysis of multilayered magneto-electro-thermoelastic strip due to uniform heat supply. Composite Structures 68, 23–36.

Pan, E., 2001. Exact solution for simply supported and multilayered magneto-electro-elastic plates. ASME Journal of Applied Mechanics 68, 608–618.

Parton, V.Z., Kudryavtsev, B.A., 1988. Electromagnetoelasticity, Piezoelectrics and Electrically Conductive Solids. Gordon & Breach Science Publishers, New York.

Sellountos, E.J., Vavourakis, V., Polyzos, D., 2005. A new singular/hypersingular MLPG (LBIE) method for 2D elastostatics. CMES: Computer Modeling in Engineering & Sciences 7, 35–48.

Sladek, J., Sladek, V., Atluri, S.N., 2000. Local boundary integral equation (LBIE) method for solving problems of elasticity with nonhomogeneous material properties. Computational Mechanics 24, 456–462.

Sladek, J., Sladek, V., Atluri, S.N., 2001. A pure contour formulation for meshless local boundary integral equation method in thermoelasticity. CMES: Computer Modeling in Engineering & Sciences 2, 423–434.

Sladek, J., Sladek, V., Van Keer, R., 2003a. Meshless local boundary integral equation method for 2D elastodynamic problems. International Journal for Numerical Methods in Engineering 57, 235–249.

Sladek, J., Sladek, V., Zhang, Ch., 2003b. Application of meshless local Petrov–Galerkin (MLPG) method to elastodynamic problems in continuously nonhomogeneous solids. CMES: Computer Modeling in Engineering & Sciences 4, 637–648.

Sladek, J., Sladek, V., Atluri, S.N., 2004. Meshless local Petrov–Galerkin method in anisotropic elasticity. CMES: Computer Modeling in Engineering & Sciences 6, 477–489.

Sladek, J., Sladek, V., Wen, P.H., Aliabadi, M.H., 2006a. Meshless Local Petrov–Galerkin (MLPG) method for shear deformable shells analysis. CMES: Computer Modeling in Engineering & Sciences 13, 103–118.

Sladek, J., Sladek, V., Zhang, Ch., Garcia-Sanchez, F., Wunsche, M., 2006b. Meshless local Petrov–Galerkin method for plane piezoelectricity. CMC: Computers, Materials & Continua 4, 109–118.

Sladek, J., Sladek, V., Zhang, Ch., Solek, P., Starek, L., 2007a. Fracture analyses in continuously nonhomogeneous piezoelectric solids by the MLPG. CMES: Computer Modeling in Engineering & Sciences 19, 247–262.

Sladek, J., Sladek, V., Zhang, Ch., Solek, P., 2007b. Application of the MLPG to thermo-piezoelectricity. CMES: Computer Modeling in Engineering & Sciences 22, 217–233.

Sladek, J., Sladek, V., Solek, P., Saez, A., 2008. Dynamic 3-D axisymmetric problems in continuously nonhomogeneous piezoelectric solids. International Journal of Solids and Structures 45, 4523–4542.

Song, Z.F., Sih, G.C., 2003. Crack initiation behavior in magnetoelectroelastic composite under in-plane deformation. Theoretical Applied Fracture Mechanics 39, 189–207.

Suresh, S., Mortensen, A., 1998. Fundamentals of Functionally Graded Materials. Institute of Materials, London.

Tian, W.Y., Gabbert, U., 2005. Macro-crack–micro-crack problem interaction problem in magnetoelectroelastic solids. Mechanics of Materials 37, 565–592.

Tian, W.Y., Rajapakse, R.K.N.D., 2005. Fracture analysis of magnetoelectroelastic solids by using path independent integrals. International Journal of Fracture 131, 311–335.

Tong, Z.H., Lo, S.H., Jiang, C.P., Cheung, Y.K., 2008. An exact solution for the three-phase thermo-electro-magneto-elastic cylinder model and its application to piezoelectric-magnetic fiber composites. International Journal Solids and Structures 45, 5205–5219.

Wang, B.L., Mai, Y.W., 2003. Crack tip field in piezoelectric/piezomagnetic media. European Journal of Mechanics A/Solids 22, 591–602.

Wang, B.L., Mai, Y.W., 2007. Applicability of the crack-face electromagnetic boundary conditions for fracture of magnetoelectroelastic materials. International Journal Solids and Structures 44, 387–398.

Wang, X., Shen, Y.P., 2002. The general solution of three-dimensional problems in magnetoelectroelastic media. International Journal of Engineering Sciences 40, 1069–1080.

Wang, B.L., Han, J.C., Mai, Y.W., 2006. Mode III fracture of a magnetoelectroelastic layer: exact solution and discussion of the crack face electromagnetic boundary conditions. International Journal of Fracture 139, 27–38.

Wen, P.H., Aliabadi, M.H., 2007. Meshless method with enriched radial basis functions for fracture mechanics. Structural Durability & Health Monitoring 3, 107–119.

Wen, P.H., Aliabadi, M.H., 2008. An improved meshless collocation method for elastostatic and elastodynamic problems. Communications in Numerical Methods in Engineering 24, 635–651.

Wen, P.H., Aliabadi, M.H., Liu, Y.W., 2008. Meshless method for crack analysis in functionally graded materials with enriched radial base functions. CMES: Computer Modeling in Engineering & Sciences 30, 133–147.

Zhou, Z.G., Wang, B., Sun, Y.G., 2004. Two collinear interface cracks in magneto-electro-elastic composites. International Journal of Engineering Sciences 42, 1155–1167.

Zhu, B., Qin, T.Y., 2007. Application of hypersingular integral equation method to three-dimensional crack in electromagnetothermoelastic multiphase composites. International Journal Solids and Structures 44, 5994–6012.

Zhu, X., Wang, Z., Meng, A., 1995. A functionally gradient piezoelectric actuator prepared by metallurgical process in PMN-PZ-PT system. Journal of Material Science Letters 14, 516–518.

Zhu, T., Zhang, J.D., Atluri, S.N., 1998. A local boundary integral equation (LBIE) method in computational mechanics, and a meshless discretization approaches. Computational Mechanics 21, 223–235.